

THERMODYNAMICS OF COMPLEX SOLIDS

Energetics of hydration on uranium oxide and peroxide surfaces

Xiaofeng Guo^{1,a)} , Di Wu^{2,b)d)} , Sergey V. Ushakov³, Tatiana Shvareva³, Hongwu Xu⁴, Alexandra Navrotsky^{3,c)d)}

¹Alexandra Navrotsky Institute for Experimental Thermodynamics, Washington State University, Pullman, Washington 99164, USA; and Department of Chemistry, Washington State University, Pullman, Washington 99164, USA

²Alexandra Navrotsky Institute for Experimental Thermodynamics, Washington State University, Pullman, Washington 99164, USA; Department of Chemistry, Washington State University, Pullman, Washington 99164, USA; and The Gene and Linda Voiland School of Chemical Engineering and Bioengineering, Washington State University, Pullman, Washington 99164, USA

³Peter A. Rock Thermochemistry Laboratory and NEAT ORU, University of California at Davis, Davis, California 95616, USA

⁴Earth and Environmental Sciences Division, Los Alamos National Laboratory, Los Alamos, New Mexico 87545, USA

^{a)}Address all correspondence to these authors. e-mail: x.guo@wsu.edu

^{b)}e-mail: d.wu@wsu.edu

^{c)}e-mail: anavrotsky@ucdavis.edu

^{d)}This author was an editor of this journal during the review and decision stage. For the *JMR* policy on review and publication of manuscripts authored by editors, please refer to <http://www.mrs.org/editor-manuscripts/>.

Received: 2 April 2019; accepted: 13 May 2019

Enthalpies of water adsorption on amorphous and crystalline oxides and peroxides of uranium are reported. Despite substantial structural and computational research on reactions between actinides and water, understanding their surface interactions from the energetic perspective remains incomplete. Direct calorimetric measurements of hydration energetics of nano-sized, bulk-sized UO_2 , U_3O_8 , anhydrous $\gamma\text{-UO}_3$, amorphous UO_3 , and U_2O_7 were carried out, and their integral adsorption enthalpies were determined to be -67.0 , -70.2 , -73.0 , -84.1 , -61.6 , and -83.6 kJ/mol water, with corresponding water coverages of 4.6, 4.5, 4.1, 5.2, 4.4, and 4.1 H_2O per nm^2 , respectively. These energetic constraints are important for understanding the interfacial phenomena between water and U-containing phases. Additionally, this set of data also helps predict the absorption and desorption behavior of water from nuclear waste forms or used nuclear fuels under repository conditions. There are also underlying relations for water coverage among different U compounds. These experimentally determined data can be used as benchmark values for future computational investigations.

Introduction

The interaction of uranium phases with water is an important topic as it is closely linked to nuclear fuel storage, repository research, and environmental concerns of nuclear waste contamination. Water can interact with actinides in multiple ways, including sorption, radiolysis, and hydrothermal chemical reactions, which result in numerous interesting and important phenomena.

Specifically, water may participate as a catalyst in the oxidation of U(IV) [and Pu(IV)] binary oxides where molecular oxygen alone hardly oxidizes the dioxides [1, 2, 3, 4, 5, 6, 7, 8, 9, 10]. Water also enhances the corrosion rate of actinides and associated fission products [5, 11, 12, 13, 14, 15, 16]. For instance, rates of corrosion increase greatly when metallic

plutonium is exposed to moisture instead of dry air [11, 17]. In the nuclear energy industry, water plays influential roles in the corrosion and degradation of nuclear fuel [15, 18, 19, 20], since H_2O provides energetically favorable pathways toward more soluble species, such as metastudtite, uranyl peroxide clusters, or other uranyl ions [15, 16, 21, 22, 23, 24]. Within used nuclear fuel (UNF) repositories, water also participates in multiple processes including dissolution, hydrogen production, and phase alteration [6, 25, 26, 27, 28, 29]. The fate of uranium in a nuclear plant accident is also subject to its interaction with water. For instance, during and in the aftermath of the Fukushima Daiichi nuclear disaster, UO_2 can react with high temperature steam and alkaline sea water to form complex solid phases and solutions [23, 30, 31]. One of the current

research efforts in nuclear industry is to develop accident-tolerant fuels such as U–Si phases [32]. Furthermore, water contributes significantly to the formation of many uranyl minerals as weathering products [33]. The chemical and physical sorption of water onto and into minerals and actinide-mineral surface reactivity in aqueous solution are also important [34, 35]. In addition, in the hydrothermal geological settings, water facilitates the alteration of uranium minerals [20, 36, 37], such as the generation of uranyl oxyhydroxides and peroxides in natural U deposits [18, 20, 21, 38, 39].

Because of the daunting issues and needs stated above, investigations of the influence of water on actinide oxides and their potential reactions have increased rapidly during the past decades from both experimental and computational perspectives. Computational techniques can provide insights about the structures and energetics of actinide dioxide–water interfaces [14, 40, 41, 42, 43, 44, 45, 46, 47], which were also studied by advanced structural characterization techniques in recent years [7, 8, 9, 10, 48, 49, 50, 51, 52]. However, related experimental thermodynamic investigations [43, 52, 53] are still scant. A solid set of calorimetric data about surface interactions is therefore of great importance in (i) serving as experimentally determined benchmarks for future computational studies and (ii) illustrating how water starts interacting with UNF and U-based nuclear wastes under a variety of geological environments.

Thus, in this work, we performed direct calorimetric measurements of water adsorption on the surfaces of UO_2 , anhydrous $\gamma\text{-UO}_3$, amorphous UO_3 , and amorphous U_2O_7 at room temperature, using a microcalorimeter coupled with a gas adsorption analyzer. Among these samples, we placed a special emphasis on UO_2 due to the significant relevance of its hydration energetics in the storage of UO_2 -based fuels and raw materials, and the permanent disposal of UNF. Previously, its isostructural (fluorite-structured) oxides, CeO_2 , $\text{Ce}_{1-x}\text{U}_x\text{O}_{2+\delta}$ and ThO_2 have been studied computationally [43, 52], and HfO_2 , ZrO_2 , CeO_2 , $\text{Ce}_{1-x}\text{U}_x\text{O}_{2+\delta}$, and UO_2 have been investigated using calorimetry [52, 54, 55]. Uranyl-containing oxides, unlike UO_2 , containing highly soluble uranyl ions and are much more susceptible to the release of radionuclides into the environment. Last, amorphous uranyl phases, mostly originating from the thermal deposition of studdite or metastuddite, can also provide pathways for mobilizing uranium in the form of uranyl species from the corroded surface of UNF [15, 16, 21, 56]. For instance, metastuddite and amorphous U_2O_7 have been discovered as products of the alteration of UNF or from precipitation during mining and storage [16, 18, 22, 56].

The samples in the present study cover almost all important basic uranium-containing phases encountered in the nuclear industry. We report hydration energetics measured

by water adsorption calorimetry to address the following three questions: (i) what are the enthalpies of water–uranium oxides interfacial interactions? (ii) what are the differences among the phases? and (iii) how do intrinsic structural variations and/or surface chemistry govern such differences?

Results and discussion

Table I summarizes the measured data. The surface area of anhydrous $\gamma\text{-UO}_3$, 1.7 m^2/g , is close to those of bulk UO_2 and U_3O_8 , 1.5 and 3.0 m^2/g , respectively. Nano-sized UO_2 has a much larger surface area (57.9 m^2/g). The amorphous compounds (am-UO_3 , $\text{am-U}_2\text{O}_7$) have similar surface areas, 8.5, and 8.8 m^2/g , respectively. We noticed that these decomposed phases have larger surface areas by 7–11% compared to that of metastuddite, and almost quadruple those values of other bulk-sized uranium oxides. All three U(VI)-containing oxides show large values of water adsorption enthalpies for the first dose at near zero coverage: –156.1, –125.1, and –202.9 kJ/mol water, for $\gamma\text{-UO}_3$, am-UO_3 , and U_2O_7 , respectively. Generally, the enthalpy of adsorption becomes less exothermic as water coverage increases (see Figs. 1–3). In the adsorption enthalpy curves, as the water coverage increases,

TABLE I: Integral enthalpies of water adsorption (Δh_{ads}) on U-containing compounds.

Sample	Surface area (m^2/g)	Coverage (H_2O per nm^2)	Δh_{ads} (kJ/mol)
$\text{am-U}_2\text{O}_7$	8.8 ± 0.1	4.1	–83.6
am-UO_3	8.5 ± 0.6	4.4 ± 0.5	-61.6 ± 6.7
$\gamma\text{-UO}_3$	1.7 ± 0.1	5.2 ± 0.6	-84.1 ± 1.1
U_3O_8	3.0 ± 0.1	4.1 ± 0.4	-73.0 ± 1.4
Bulk- UO_2	1.5 ± 0.1	4.5 ± 0.1	-70.2 ± 1.2
Nano- UO_2	57.9 ± 0.2	4.6	–67.0

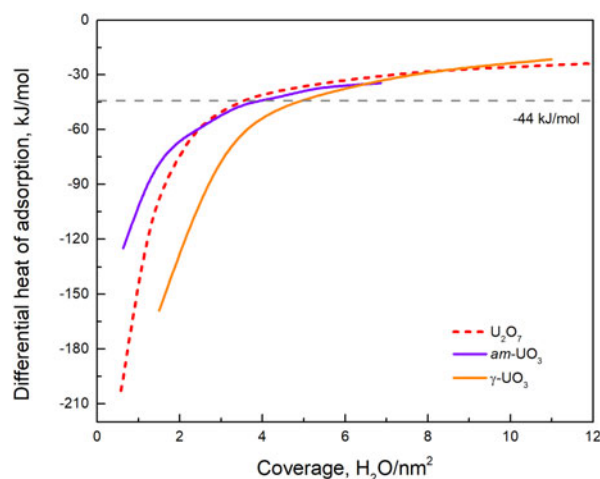


Figure 1: Differential enthalpies of water adsorption (Δh_{ads}) as a function of water coverage on U^{6+} -containing compounds.

differential enthalpies of water adsorption (Δh_{ads}) at -44 kJ/mol water define the end of the investigation of adsorbed water on these samples. This is because -44 kJ/mol water is the heat released when water vapor condenses to the liquid phase at 25 °C. If the hydration energy appears less exothermic than -44 kJ/mol water, it is very likely that additional dosed water molecules barely interact with the sample surface, rather tending to self-interact by forming clusters [57, 58]. Such behavior is not relevant to the present study and will not be further discussed. Thus, we can derive the integral water adsorption enthalpy by integrating all Δh_{ads} smaller than -44 kJ/mol and the obtained results are shown in Table I.

Starting from UO_2 , increasing the valence of U will be accommodated by excess oxygen existing as clusters in the interstitial sites of the fluorite structure till the formation of intermediate phases, such as U_3O_7 and U_4O_9 [59, 60]. Exceeding $\text{O}/\text{U} = 2.33$ will break the fluorite-derived arrangement of cations and lead to the emergence of U_3O_8 phase [60, 61]. Such oxidizing transitions are the combination of diffusion-controlled processes and nucleation reactions, which has impacts on the hydration energetics of the forming phases. Moving from tetravalent U to mixed valence states, then to hexavalent U, the hydration profiles of the crystalline oxide phases (UO_2 , U_3O_8 , and UO_3) shift accordingly (Fig. 1), with an increasingly exothermic trend. Compared with U^{4+} in UO_2 , U^{5+} and/or U^{6+} in U_3O_8 and UO_3 provide increased electronic attractions to the negatively charged oxygen in water molecules, leading to more stable U–O bonding [60, 62]. Particularly, the integral enthalpy of water adsorption of UO_2 is -70.2 ± 1.2 kJ/mol water, relatively close to that of CeO_2 (-59.8 ± 0.7 kJ/mol water) or ThO_2 (-65.0 ± 1.2 kJ/mol water) [43], both of which also crystallize in the fluorite structure, but Ce or Th cannot be further oxidized.

The oxidation of UO_2 in humid conditions may result in oxidation of the near surface (up to $1 \mu\text{m}$) and/or formation of surface hydroxyls, observed by XPS and Raman spectroscopy [7, 8, 48, 49]. Water vapor alone has only minimal (catalytic) impacts on the surface oxidation of UO_2 [10, 14, 59]. In Fig. 2, there is a relatively sharp transition of the differential enthalpy of adsorption curve of UO_2 from overlapping that of U_3O_8 (step i) to that of $\gamma\text{-UO}_3$ (step ii). U_3O_8 is the weathering product of uraninite and it is kinetically and thermodynamically stable. Previously, it has shown that the oxidation and hydration of U_3O_8 to schoepite can occur only after long storage time (2–3.5 years) in humidity [63], suggestive of a very slow reaction rate. Therefore, U_3O_8 samples under current experimental periods should not have any noticeable bulk-scale structural alterations. Thus, we conclude before the coverage of 3 water per nm^2 , water adsorption on UO_2 behaves similarly to that on the reduced U oxide. Suggested by DFT calculations

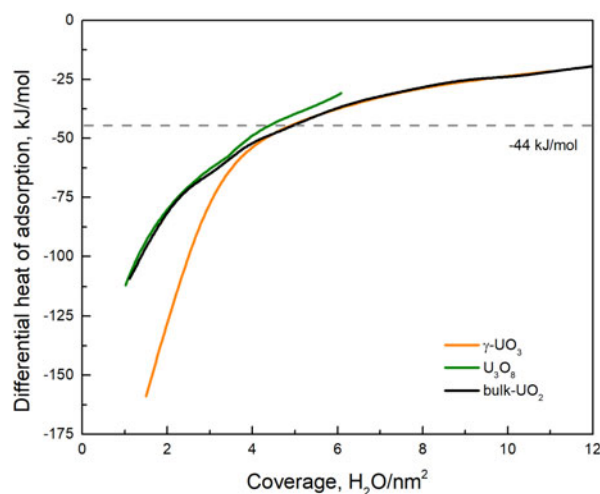


Figure 2: Comparison of differential enthalpies of water adsorption and water coverages among $\gamma\text{-UO}_3$, U_3O_8 , and UO_2 .

and experimental observations, the (111) surface of UO_2 has the lowest surface energy [43, 44, 64, 65] that has the highest possibility to stabilize the molecular or dissociated water molecules. Thus, the interaction enthalpy from the initial water dosage $\Delta h_{\text{ads}} = -103.4 \pm 7.7$ kJ/mol can be attributed to the interaction between the (111) surface and water consistent with calculated results ($-90.7 \sim -106.1$ kJ/mol) [43, 44, 45, 46]. The difference may be due to the energetic contributions from other planes or defective adsorption sites. U_3O_8 can be viewed as the high temperature phase resulting from the shear transformation of the UO_2 lattice along the (111) planes [61, 66]. Thus, UO_2 and U_3O_8 have similar atomic arrangements in (111) layers which could lead to the similarity in adsorption behavior and integral water adsorption enthalpies (-70.2 versus -73.0 kJ/mol). However, as the water coverage increases into the “step 2” regime, additional water molecules may interact with the altered surface modified by previous adsorbed water that comprised higher valence U and hydroxyl groups, which could resemble the surface of $\gamma\text{-UO}_3$ under the same water coverage (Fig. 2). Therefore, the measured water adsorption enthalpy of UO_2 , $\Delta h_{\text{ads}} = -70.2 \pm 1.2$ kJ/mol, includes the energetic terms from the oxidation of U^{4+} and the interaction of water with modified surfaces. This explains that why $\Delta h_{\text{ads}}(\text{UO}_2)$ is higher than that of CeO_2 (-59.8 ± 0.7 kJ/mol) [55] or ThO_2 (-65.0 ± 1.2 kJ/mol) [43], where Ce^{4+} and Th^{4+} cannot be further oxidized. The Δh_{ads} of UO_2 from this work is also consistent with a recently published Δh_{ads} of $\text{UO}_{2+\delta}$ by Shelly et al. (-68 ± 7 kJ/mol) [52]. The observation of stepwise behavior is consistent with previous reports on the humidity-dependent influence of water vapor on the surface of UO_2 where three processes were identified in the alteration of fresh UO_2 fuel under aerated water and high-temperature conditions [67].

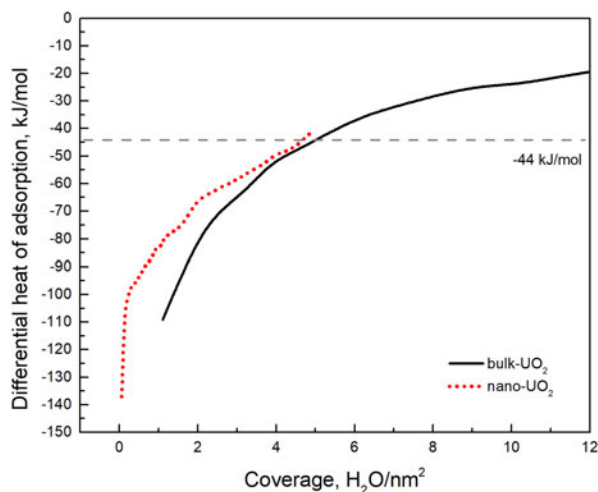


Figure 3: Differential enthalpies of water adsorption as a function of water coverage on bulk- UO_2 and nano- UO_2 .

For nano-sized UO_2 , the enthalpy of water adsorption for the first dose is almost 30 kJ/mol more exothermic than for bulk UO_2 (-137.1 kJ/mol), presumably due to the much higher surface area with more distributed defects and active sites available for bonding. Yet there is a convergence of their adsorption curves at -44 kJ/mol that yields similar water coverages before condensation (Fig. 3): 4.5 and 4.6 H_2O per nm^2 for bulk-sized and nano-sized UO_2 , respectively. This could suggest that despite having a higher surface area, nano- UO_2 still has a hydrophobic surface; and after saturating all active sites by water molecules, the continuing adsorption behavior after around 5 H_2O per nm^2 coverage will be similar between nano- and bulk- UO_2 . Therefore, the hydration process of nano- UO_2 may not differ too much from its bulk counterpart under a high humidity environment.

Conclusions

In this work, we performed direct calorimetric measurements of hydration energetics of nano-sized, bulk-sized UO_2 , U_3O_8 , anhydrous $\gamma\text{-UO}_3$, amorphous UO_3 , and U_2O_7 , and obtained their water adsorption enthalpies to be -67.0 , -70.2 , -73.0 , -84.1 , -61.6 , and -83.6 kJ/mol water, with water coverage of 4.6, 4.5, 4.1, 5.2, 4.4, and 4.1 H_2O per nm^2 , respectively. Particularly, the hydration behavior of UO_2 was deconvoluted to a two-step process with the first part overlapping that of U_3O_8 then transiting to the second part resembling that of $\gamma\text{-UO}_3$. The difference between hydration energetics of nano- and bulk- UO_2 resides mostly in low water coverages and diminishes at high water coverages where the two water adsorption energetic profiles converge, which indicates the hydration of UO_2 in the environment over the long term is less dependent of the particle size.

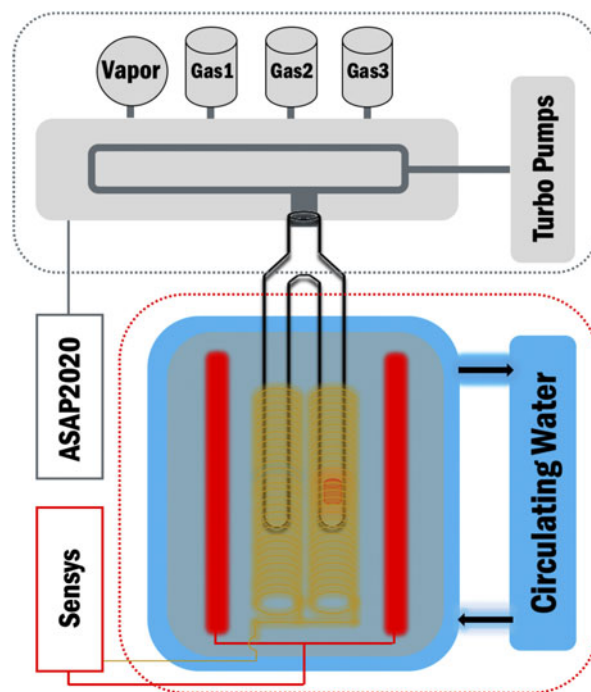


Figure 4: Schematics of gas/water adsorption calorimetry by coupling Calvet-type microcalorimeter with a gas dosing and adsorption analyzer.

Methods and approaches

The calorimetric experiments were accomplished by a gas adsorption calorimetric method using a Calvet-type microcalorimeter unit (Setaram Sensys) coupled with a commercial gas adsorption analyzer with a gas dosing system (Micromeritics ASAP 2020, Micromeritics, Norcross, Georgia) [58, 68] (see Fig. 4). The experiments were performed in four steps. First, a ~ 80 mg sample was placed in a silica-glass forked tube and degassed under vacuum ($<10^{-3}$ Pa) for 24 h using the Micromeritics ASAP 2020 instrument. Second, the free space of the sample tube and the surface of the sample were determined by Brunauer–Emmett–Teller (BET) analysis of nitrogen, argon or krypton adsorption. Third, the forked tube was inserted into the calorimeter at 25°C , and water adsorption experiments were programmed with the Micromeritics instrument using $1\ \mu\text{mol}$ of water vapor dose amounts and 1.5 h equilibration time after each dose. The actual adsorbed amounts were obtained from the measured adsorption isotherm. Each dose produced an exothermic peak recorded by the calorimeter software. The integration of the peak provided the enthalpy of adsorption for each dose using a calibration factor based on the enthalpy of fusion of gallium.

The degas temperature prior to the adsorption experiments was selected to retain the structure of studied samples. The UO_2 sample, confirmed to be stoichiometric, was provided by Los Alamos National Laboratory. $\gamma\text{-UO}_3$ and U_3O_8 were obtained from International Bio-Analytical Industries. *am-*

UO_3 and U_2O_7 were obtained by the thermal decomposition of metastudtite [16, 56]. Preheating and degassing treatments were performed in the forked tube using the Micromeritics instrument. UO_2 and U_3O_8 samples were degassed at 400 °C for 4 h. Anhydrous UO_3 was formed by heating hydrated UO_3 and degassing at 350 °C for 5 h *am*- U_2O_7 and *am*- UO_3 were pretreated at 80 °C for 5 h in vacuum.

Acknowledgments

This work was supported by the Materials Science of Actinides (MSA), an Energy Frontier Research Center (EFRC), funded by the U.S. Department of Energy, Office of Science, Office of Basic Energy Sciences under Award Number DE-SC0001089, and the Laboratory Directed Research and Development (LDRD) program (Project #20180007 DR) of Los Alamos National Laboratory (LANL). We thank Peter Burns for his support of this work through leading the MSA EFRC, and X.G. acknowledges support through a LANL Seaborg postdoctoral fellowship and, later, institutional funds from the Department of Chemistry at Washington State University. D.W. was also supported by the institutional funds from the Gene and Linda Voiland School of Chemical Engineering and Bioengineering at Washington State University. D.W. and X.G. acknowledge the fund of Alexandra Navrotsky Institute for Experimental Thermodynamics. LANL, an affirmative action/equal opportunity employer, is managed by Triad National Security, LLC, for the National Nuclear Security Administration of the U.S. Department of Energy under contract 89233218CNA000001.

References

1. T.E. Eriksen, U.B. Eklund, L. Werme, and J. Bruno: Dissolution of irradiated fuel: A radiolytic mass balance study. *J. Nucl. Mater.* **227**, 76 (1995).
2. D.J. Wronkiewicz, J.K. Bates, S.F. Wolf, and E.C. Buck: Ten-year results from unsaturated drip tests with UO_2 at 90 °C: Implications for the corrosion of spent nuclear fuel. *J. Nucl. Mater.* **238**, 78 (1996).
3. S. Sunder, D.W. Shoesmith, and N.H. Miller: Oxidation and dissolution of nuclear fuel (UO_2) by the products of the alpha radiolysis of water. *J. Nucl. Mater.* **244**, 66 (1997).
4. H. Christensen and S. Sunder: Current state of knowledge of water radiolysis effects on spent nuclear fuel corrosion. *Nucl. Technol.* **131**, 102 (2000).
5. J.M. Haschke, T.H. Allen, and L.A. Morales: Reaction of plutonium dioxide with water: Formation and properties of PuO_{2+x} . *Science* **287**, 285 (2000).
6. J.A. La Verne and L. Tandon: H_2 production in the radiolysis of water on UO_2 and other oxides. *J. Phys. Chem. B* **107**, 13623 (2003).
7. S.D. Senanayake, G.I.N. Waterhouse, A.S.Y. Chan, T.E. Madey, D.R. Mullins, and H. Idriss: Probing surface oxidation of reduced uranium dioxide thin film using synchrotron radiation. *J. Phys. Chem. C* **111**, 7963 (2007).
8. S.D. Senanayake, G.I.N. Waterhouse, A.S.Y. Chan, T.E. Madey, D.R. Mullins, and H. Idriss: The reactions of water vapour on the surfaces of stoichiometric and reduced uranium dioxide: A high resolution XPS study. *Catal. Today* **120**, 151 (2007).
9. H. Idriss: Surface reactions of uranium oxide powder, thin films and single crystals. *Surf. Sci. Rep.* **65**, 67 (2010).
10. S.B. Donald, Z.R. Dai, M.L. Davisson, J.R. Jeffries, and A.J. Nelson: An XPS study on the impact of relative humidity on the aging of UO_2 powders. *J. Nucl. Mater.* **487**, 105 (2017).
11. J.M. Haschke, T.H. Allen, and L.A. Morales: Surface and corrosion chemistry of plutonium. *Los Alamos Sci.* **26**, 252 (2000).
12. H.W. Xu, A. Navrotsky, M.D. Nyman, and T.M. Nenoff: Thermochemistry of microporous silicotitanate phases in the Na_2O - Cs_2O - SiO_2 - TiO_2 - H_2O system. *J. Mater. Res.* **15**, 815 (2000).
13. M.L. Balmer, Y. Su, H. Xu, E. Bitten, D. McCready, and A. Navrotsky: Synthesis, structure determination, and aqueous durability of $\text{Cs}_2\text{ZrSi}_3\text{O}_9$. *J. Am. Ceram. Soc.* **84**, 153 (2001).
14. F.N. Skomurski, L.C. Shuller, R.C. Ewing, and U. Becker: Corrosion of UO_2 and ThO_2 : A quantum-mechanical investigation. *J. Nucl. Mater.* **375**, 290 (2008).
15. X. Guo, S.V. Ushakov, S. Labs, H. Curtius, D. Bosbach, and A. Navrotsky: Energetics of metastudtite and implications for nuclear waste alteration. *Proc. Natl. Acad. Sci. U.S.A.* **111**, 17737 (2014).
16. X. Guo, D. Wu, H. Xu, P.C. Burns, and A. Navrotsky: Thermodynamic studies of studtite thermal decomposition pathways via amorphous intermediates UO_3 , U_2O_7 , and UO_4 . *J. Nucl. Mater.* **478**, 158 (2016).
17. R.G. Haire and J.M. Haschke: Plutonium oxide systems and related corrosion products. *MRS Bull.* **26**, 689 (2001).
18. G. Sattonnay, C. Ardois, C. Corbel, J.F. Lucchini, M.F. Barthe, F. Garrido, and D. Gosset: Alpha-radiolysis effects on UO_2 alteration in water. *J. Nucl. Mater.* **288**, 11 (2001).
19. B. McNamara, E. Buck, and B. Hanson: Observation of studtite and metastudtite on spent fuel. *Mater. Res. Soc. Symp. Proc.* **757**, 401 (2003).
20. X. Guo, S. Szenknect, A. Mesbah, S. Labs, N. Clavier, C. Poinssot, S.V. Ushakov, H. Curtius, D. Bosbach, R.C. Ewing, P.C. Burns, N. Dacheux, and A. Navrotsky: Thermodynamics of formation of coffinite, USiO_4 . *Proc. Natl. Acad. Sci. U.S.A.* **112**, 6551 (2015).
21. K.A.H. Kubatko, K.B. Helean, A. Navrotsky, and P.C. Burns: Stability of peroxide-containing uranyl minerals. *Science* **302**, 1191 (2003).
22. B. Hanson, B. McNamara, E. Buck, J. Friese, E. Jenson, K. Krupka, and B. Arey: Corrosion of commercial spent nuclear fuel. 1. Formation of studtite and metastudtite. *Radiochim. Acta* **93**, 159 (2005).

23. C.R. Armstrong, M. Nyman, T. Shvareva, G.E. Sigmon, P.C. Burns, and A. Navrotsky: Uranyl peroxide enhanced nuclear fuel corrosion in seawater. *Proc. Natl. Acad. Sci. U.S.A.* **109**, 1874 (2012).
24. E. Tiferet, A. Gil, C. Bo, T.Y. Shvareva, M. Nyman, and A. Navrotsky: The energy landscape of uranyl-peroxide species. *Chem.–Eur. J.* **20**, 3646 (2014).
25. P. Taylor, R.J. Lemire, and D.D. Wood: The influence of moisture on air oxidation of UO_2 —Calculations and observations. *Nucl. Technol.* **104**, 164 (1993).
26. M. Abramowski, S.E. Redfern, R.W. Grimes, and S. Owens: Modification of UO_2 crystal morphologies through hydroxylation. *Surf. Sci.* **490**, 415 (2001).
27. M. Jonsson, F. Nielsen, O. Roth, E. Ekeröth, S. Nilsson, and M.M. Hossain: Radiation induced spent nuclear fuel dissolution under deep repository conditions. *Environ. Sci. Technol.* **41**, 7087 (2007).
28. C. Jegou, R. Caraballo, J. De Bonfils, V. Broudic, S. Peugeot, T. Vercouter, and D. Roudil: Oxidizing dissolution of spent MOX47 fuel subjected to water radiolysis: Solution chemistry and surface characterization by Raman spectroscopy. *J. Nucl. Mater.* **399**, 68 (2010).
29. A. Timofeev, A.A. Migdisov, A.E. Williams-Jones, R. Roback, A.T. Nelson, and H. Xu: Uranium transport in acidic brines under reducing conditions. *Nat. Commun.* **9**, 1469 (2018).
30. B. Grambow and C. Poinssot: Interactions between nuclear fuel and water at the Fukushima Daiichi reactors. *Elements* **8**, 213 (2012).
31. P.C. Burns, R.C. Ewing, and A. Navrotsky: Nuclear fuel in a reactor accident. *Science* **335**, 1184 (2012).
32. X. Guo, J.T. White, A.T. Nelson, A. Migdisov, R. Roback, and H. Xu: Enthalpy of formation of U_3Si_2 : A high-temperature drop calorimetry study. *J. Nucl. Mater.* **507**, 44 (2018).
33. R. Finch and T. Murakami: Systematics and paragenesis of uranium minerals. *Rev. Mineral.* **38**, 152 (1999).
34. A.S. Icenhour, L.M. Toth, and H.M. Luo: Water sorption and gamma radiolysis studies for uranium oxides. *Nucl. Technol.* **147**, 258 (2004).
35. H. Geckeis, J. Lutzenkirchen, R. Polly, T. Rabung, and M. Schmidt: Mineral-water interface reactions of actinides. *Chem. Rev.* **113**, 1016 (2013).
36. J. Janeczek and R.C. Ewing: Coffinitization—A mechanism for the alteration of UO_2 under reducing conditions. In *Scientific Basis for Nuclear Waste Management XV*, Vol. 257 (Materials Research Society, Warrendale, Pennsylvania, 1992); p. 497.
37. A.P. Deditius, S. Utsunomiya, and R.C. Ewing: The chemical stability of coffinite, $\text{USiO}_4 \cdot n\text{H}_2\text{O}$; $0 < n < 2$, associated with organic matter: A case study from grants uranium region, New Mexico, USA. *Chem. Geol.* **251**, 33 (2008).
38. C. Frondel: Systematic mineralogy of uranium and thorium. *U.S. Geol. Surv. Bull.* **1064**, 400 (1958).
39. M. Deliens and P. Piret: Metastudtite, $\text{UO}_4 \cdot 2\text{H}_2\text{O}$, a new mineral from Shinkolobwe, Shaba, Zaire. *Am. Mineral.* **68**, 456 (1983).
40. A.H.H. Tan, R.W. Grimes, and S. Owens: Structures of UO_2 and PuO_2 surfaces with hydroxide coverage. *J. Nucl. Mater.* **344**, 13 (2005).
41. P.J. Hay: Theoretical studies of hydrogen and water adsorption on actinide oxide surfaces. *Mater. Res. Soc. Symp. Proc.* **893**, 1–6 (2005).
42. F.N. Skomurski, R.C. Ewing, and U. Becker: Adsorption energy trends on UO_2 and ThO_2 surfaces. *Geochim. Cosmochim. Acta* **71**, A945 (2007).
43. V. Alexandrov, T.Y. Shvareva, S. Hayun, M. Asta, and A. Navrotsky: Actinide dioxides in water: Interactions at the interface. *J. Phys. Chem. Lett.* **2**, 3130 (2011).
44. Z. Rak, R.C. Ewing, and U. Becker: Hydroxylation-induced surface stability of AnO_2 ($\text{An} = \text{U}, \text{Np}, \text{Pu}$) from first-principles. *Surf. Sci.* **608**, 180 (2013).
45. T. Bo, J.H. Lan, C.Z. Wang, Y.L. Zhao, C.H. He, Y.J. Zhang, Z.F. Chai, and W.Q. Shi: First-principles study of water reaction and H_2 formation on UO_2 (111) and (110) single crystal surfaces. *J. Phys. Chem. C* **118**, 21935 (2014).
46. P. Maldonado, L.Z. Evins, and P.M. Oppeneer: Ab initio atomistic thermodynamics of water reacting with uranium dioxide surfaces. *J. Phys. Chem. C* **118**, 8491 (2014).
47. X-f. Tian, H. Wang, H-x. Xiao, and T. Gao: Adsorption of water on UO_2 (111) surface: Density functional theory calculations. *Comput. Mater. Sci.* **91**, 364 (2014).
48. S.D. Senanayake and H. Idriss: Water reactions over stoichiometric and reduced UO_2 (111) single crystal surfaces. *Surf. Sci.* **563**, 135 (2004).
49. H. Idriss and S.D. Senanayake: Reaction of water on oxygen-defected UO_2 (111) single crystal surface. *Abstr. Pap. Am. Chem. S.* **227**, U89 (2004).
50. A. Espriu-Gascon, J. Llorca, M. Domínguez, J. Giménez, I. Casas, and J. de Pablo: UO_2 surface oxidation by mixtures of water vapor and hydrogen as a function of temperature. *J. Nucl. Mater.* **467**, 240 (2015).
51. J.E. Stubbs, A.M. Chaka, E.S. Ilton, C.A. Biwer, M.H. Engelhard, J.R. Bargar, and P.J. Eng: UO_2 oxidative corrosion by nonclassical diffusion. *Phys. Rev. Lett.* **114**, 246103 (2015).
52. L. Shelly, D. Schweke, S. Zalkind, N. Shamir, S. Barzilai, T. Gouder, and S. Hayun: Effect of U content on the activation of H_2O on $\text{Ce}_{1-x}\text{U}_x\text{O}_{2+\delta}$ surfaces. *Chem. Mater.* **30**, 8650–8660 (2018).
53. M.T. Paffett, D. Kelly, S.A. Joyce, J. Morris, and K. Veirs: A critical examination of the thermodynamics of water adsorption on actinide oxide surfaces. *J. Nucl. Mater.* **322**, 45 (2003).
54. S.V. Ushakov and A. Navrotsky: Direct measurements of water adsorption enthalpy on hafnia and zirconia. *Appl. Phys. Lett.* **87**, 164103 (2005).
55. S. Hayun, T.Y. Shvareva, and A. Navrotsky: Nanocerium—Energetics of surfaces, interfaces and water adsorption. *J. Am. Ceram. Soc.* **94**, 3992 (2011).

56. S.O. Odoh, J. Shamblin, C.A. Colla, S. Hickam, H.L. Lobeck, R.A.K. Lopez, T. Olds, J.E.S. Szymanowski, G.E. Sigmon, J. Neuefeind, W.H. Casey, M. Lang, L. Gagliardi, and P.C. Burns: Structure and reactivity of X-ray amorphous uranyl peroxide, U_2O_7 . *Inorg. Chem.* **55**, 3541 (2016).
57. D. Wu, X. Guo, H. Sun, and A. Navrotsky: Energy landscape of water and ethanol on silica surfaces. *J. Phys. Chem. C* **119**, 15428 (2015).
58. G. Li, H. Sun, H. Xu, X. Guo, and D. Wu: Probing the energetics of molecule–material interactions at interfaces and in nanopores. *J. Phys. Chem. C* **121**, 26141 (2017).
59. R.J. McEachern and P. Taylor: A review of the oxidation of uranium dioxide at temperatures below 400 °C. *J. Nucl. Mater.* **254**, 87 (1998).
60. G. Leinders, R. Bes, J. Pakarinen, K. Kvashnina, and M. Verwerft: Evolution of the uranium chemical state in mixed-valence oxides. *Inorg. Chem.* **56**, 6784 (2017).
61. L. Desgranges, G. Baldinozzi, D. Simeone, and H. Fischer: Refinement of the α - U_4O_9 crystalline structure: New insight into the $U_4O_9 \rightarrow U_3O_8$ transformation. *Inorg. Chem.* **50**, 6146 (2011).
62. K. Kvashnina, S.M. Butorin, P. Martin, and P. Glatzel: Chemical state of complex uranium oxides. *Phys. Rev. Lett.* **111**, 253002 (2013).
63. A.L. Tamasi, K.S. Boland, K. Czerwinski, J.K. Ellis, S.A. Kozimor, R.L. Martin, A.L. Pugmire, D. Reilly, B.L. Scott, A.D. Sutton, G.L. Wagner, J.R. Walensky, and M.P. Wilkerson: Oxidation and hydration of U_3O_8 materials following controlled exposure to temperature and humidity. *Anal. Chem.* **87**, 4210 (2015).
64. G. Allen, P. Tempest, and J. Tyler: The formation of U_3O_8 on crystalline UO_2 . *Philos. Mag. B* **54**, L67 (1986).
65. G.C. Allen, P.A. Tempest, and J.W. Tyler: Oxidation of crystalline UO_2 studied using X-ray photoelectron spectroscopy and X-ray diffraction. *J. Chem. Soc., Faraday Trans. 1* **83**, 925 (1987).
66. G. Allen and N. Holmes: A mechanism for the UO_2 to α - U_3O_8 phase transformation. *J. Nucl. Mater.* **223**, 231 (1995).
67. P. Taylor, D.D. Wood, D.G. Owen, and G-I. Park: Crystallization of U_3O_8 and hydrated UO_3 on UO_2 fuel in aerated water near 200 °C. *J. Nucl. Mater.* **183**, 105 (1991).
68. S.V. Ushakov, N. Dalalo, and A. Navrotsky: Gas adsorption microcalorimetry: Probing energetics of oxide surfaces. *Geochim. Cosmochim. Acta* **69**, A485 (2005).